THE JOURNAL OF PHYSICAL CHEMISTRY Letters

Letter

Cite This: J. Phys. Chem. Lett. 2019, 10, 3820−3827

pubs.acs.org/JPCL

Decreasing Exciton Binding Energy in Two-Dimensional Halide Perovskites by Lead Vacancies

Yurui Gao,[†] Mingliang Zhang,[‡] Xu Zhang,[†] and Gang Lu*[,†]

[†]Department of Physics and Astronomy, California State University, Northridge, Northridge, California 91330-8268, United States

[‡]Beijing Computational Science Research Center, Beijing 100193, China

Supporting Information

ABSTRACT: Two-dimensional (2D) perovskites, such as $(BA)_2(MA)_{n-1}Pb_nX_{3n+1}$ (X = Cl, Br, or I), have shown great promise in optoelectronic applications because of their stability, tunability, and unique electronic properties. However, their photovoltaic applications are hindered by high exciton binding energies in phases when n is small. On the basis of first-principles calculations, we predict that the exciton binding energy in the atomically thin 2D perovskites (n = 1 and 2) can be decreased significantly by neutral lead vacancies so that free charge carriers can be readily generated at room temperature. Moreover, the photogenerated electrons and holes are delocalized and spatially separated in the presence of lead vacancies; hence, radiative charge recombination can be suppressed. The lead vacancies are predicted to be formed in the 2D perovskites in an I-rich synthetic environment. Some intriguing experimental observations may be related to the presence of lead vacancies in the 2D perovskites.

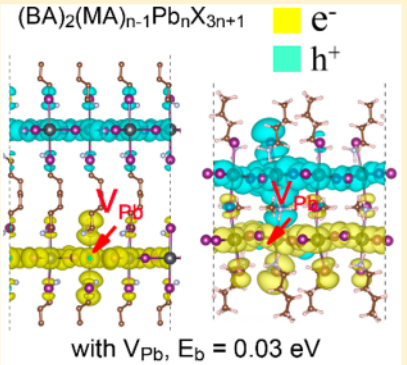

Hybrid organic−inorganic halide perovskites have emerged as some of the most promising materials for optoelectronic applications, including photovoltaics, photodetectors, and light-emitting diodes, because of their low fabrication costs and high performance.[1−11] In only a few years, the power conversion efficiencies (PCEs) of three-dimensional (3D) lead halide perovskites have exceeded 23.7%,[12,13] generating tremendous excitement in the scientific and technological communities. Despite the excitement, however, these 3D perovskites suffer from critical stability problems; they are sensitive to water moisture, ultraviolet light, and thermal stress,[6,14−17] which represents a major roadblock to their commercialization. On the other hand, two-dimensional (2D) lead halide perovskites have recently been shown to exhibit superior stability and water resistance relative to their 3D counterparts.[18−21] Solar cells based on the 2D perovskites, such as $(BA)_2(MA)_{n-1}Pb_nX_{3n+1}$ ($BA = C_4H_9NH_3^+$, butylammonium cation; $MA = CH_3NH_3^+$, methylammonium cation; X = Cl, Br, or I), have exhibited a PCE of 12.5%.[22] In addition, solar cells with a combination of 2D/3D perovskites have achieved 17.5% efficiency. More impressively, they can sustain 80% of their "post burn-in" efficiencies after 1000 h in air and 4000 h when encapsulated.[23,24]

The 2D perovskites comprise variable inorganic slabs separated by organic ammonium cations and can be considered as multiple quantum wells, with the inorganic slabs acting as "wells" and the organic spacer as "barriers". As a result, the 2D perovskites can offer much broader structural versatility and optoelectronic tunability than either their 3D counterparts or the traditional quantum dots.[25−29] More specifically, the optical band gap (E_{opt}) and the exciton binding energy (E_b) of the 2D perovskites can be tuned by varying the thickness of the inorganic slabs or n value.[18,25,26,30,31] For example, as n decreases from 4 to 1 in $(BA)_2(MA)_{n-1}Pb_nI_{3n+1}$, E_{opt} increases monotonically from 1.9 to 2.5 eV and E_b from 0.12 to 0.43 eV.[31−33] In particular, for atomically thin 2D perovskites for which n = 1−3, E_b is much larger than the room-temperature thermal fluctuation (K_BT = 0.026 eV at 300 K). As a comparison, E_b in the 3D perovskites (e.g., $MAPbI_3$) is ∼0.06 eV.[34−37] The much stronger exciton binding in the 2D perovskites can be attributed to the prominent quantum and dielectric confinement effect manifested in the lower-dimensional materials.[38] The fact that E_b is much larger than K_BT dictates that the photogenerated electrons and holes are strongly bound in the 2D perovskites; thus, free carrier generation is significantly suppressed. This is a particularly severe problem in atomically thin 2D perovskites (n = 1 or 2) in which the exciton binding energy is the highest. It is unfortunate because the atomically thin 2D perovskites are among the most appealing materials and would otherwise be highly attractive for photovoltaic applications. From a practical point of view, it is very challenging to produce phase-pure (a single n value) 2D perovskites with low-cost fabrications; thus, perovskite phases with smaller n values may be unavoidable. Although the band gaps of the atomically thin 2D perovskites are not ideal, recent density functional theory (DFT) calculations based on the hybrid functional and spin−orbit coupling (SOC) have shown that 2D $(BA)_2PbX_4$ (X = Cl, Br,

Received: April 16, 2019
Accepted: June 21, 2019
Published: June 21, 2019

DOI: 10.1021/acs.jpclett.9b01093
J. Phys. Chem. Lett. 2019, 10, 3820−3827

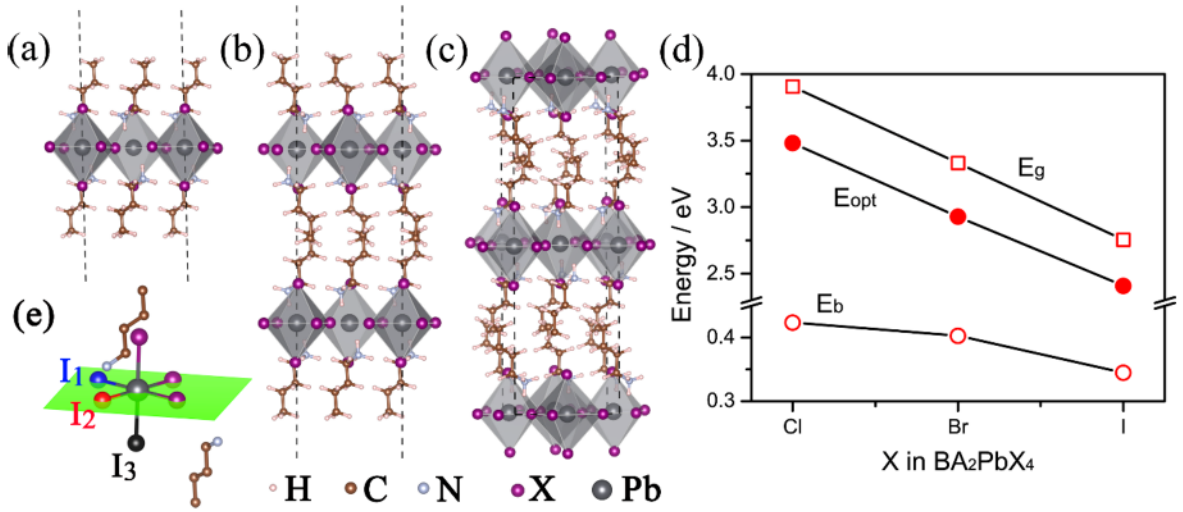

Figure 1. Primitive unit cells of the (a) SL, (b) DL, and (c) bulk phase of $(BA)_2PbX_4$ (X = Cl, Br, or I). (d) Calculated band gaps and exciton binding energy for bulk $(BA)_2PbX_4$. (e) Three non-equivalent I sites involved in the point defects.

or I) perovskites exhibit strong optical transitions in the range of visible light, and optical absorption tuning can be achieved by varying their chemical compositions and layer thicknesses.[39] Other intriguing properties associated with the 2D perovskites, such as their 2D nature, versatility, tunability, and stability, also make them attractive for photovoltaics. Therefore, it would be of great scientific and technological interest to discover a means of decreasing the exciton binding energy in the atomically thin 2D perovskites. Because defect engineering is one of the most effective and broadly used approaches to modulate the properties of semiconductors, we will explore in this work whether and how point defects may change the optoelectronic properties of the atomically thin 2D perovskites. Using a newly developed first-principles method, we are able to examine excitonic properties in defective 2D perovskites using supercells much larger than what were previously feasible. In particular, we predict that neutral lead vacancies can decrease E_b in bulk $(BA)_2(MA)_{n-1}Pb_nI_{3n+1}$ (n = 1 or 2) to ~0.03 eV. The photoexcited electrons and holes are found to be spatially separated and delocalized, suppressing charge recombination in the 2D perovskites.

The conventional first-principles approach to determining the optoelectronic and excitonic properties of semiconductors is the so-called GW-Bethe-Salpeter equation (GW-BSE) method based on the many-body perturbation theory.[40−42] Although it is very accurate, the GW-BSE method is computationally too expensive to deal with large supercells as required to model defects. In this work, we employ a newly developed first-principles approach,[43−45] which is based on time-independent density functional theory and time-dependent density functional theory (TDDFT) with optimally tuned and range-separated hybrid exchange-correlation functionals (OT-RSH).[46−48] The (TD)DFT-OT-RSH method is computationally much more expedient than the GW-BSE approach and can treat thousands of atoms in a supercell. In our (TD)DFT-OT-RSH calculations, only the Gamma point in the Brillouin zone is sampled in conjunction with employing large supercells. The Perdew−Burke−Ernzerhof (PBE) functional[49] with Grimme's D2 dispersion correction[50] is used to capture the van der Waals interaction in the perovskites. More details about the (TD)DFT-OT-RSH method and the computational parameters employed can be found in the Supporting Information.

We first examine the properties of the pristine $(BA)_2PbI_4$, including the single-layer (SL), double-layer (DL), and bulk phase (panels a−c of Figure 1, respectively). The lattice parameters of the bulk phase are found to be a = 8.60 Å, b = 8.53 Å, and c = 27.09 Å (Table 1S), which are close to the experimental values of a = 8.86 Å, b = 8.68 Å, and c = 27.57 Å,[51] thus validating the D2 dispersion correction used in the calculations. The static dielectric constant (ε_0) is a key material quantity that is calculated for the bulk phase using the density functional perturbation theory (DFPT) (results in Table 1S). The average in-plane component of ε_0 is estimated to be 9.3, much larger than its out-of-plane component of 4.4, as expected. These numbers agree well with the previously reported values (9.5 and 4.0).[52] As the halogen varies from Cl to I, the average dielectric constant increases (6.72, 6.86, and 7.63 for Cl, Br, and I, respectively). Clearly, the dielectric constants of the 2D perovskites are much smaller than those of the 3D counterparts (e.g., ε_0 = 22−37 in $MAPbI_3$).[34,52−54] In addition, we have calculated ε_0 for both orthorhombic and tetrahedral phases of $MAPbI_3$ and the results (20.63 and 22.72) agree well with the quoted values.

The (TD)DFT-OT-RSH approach has been used successfully to determine the optoelectronic and excitonic properties of ionic insulators, organic and inorganic semiconductors, 3D perovskites, and 2D materials (graphene fluoride and phosphorene) with and without point defects.[45−48,55,56] In this work, we first carry out DFT-OT-RSH calculations to obtain the fundamental band gap (E_g) of the pristine $(BA)_2PbI_4$ with a choice of α, β, and γ values ($\beta = \varepsilon_0^{-1} - \alpha$). We next vary α, β, and γ values (using the dielectric constants obtained above) until the computed E_g matches the experimental value of 2.73 eV.[32] In this way, we determine α = 0.1 (β = 0.031) and γ = 0.57 $Å^{-1}$. With this set of parameters, we subsequently perform TDDFT-OT-RSH calculations without spin−orbital coupling (SOC) to estimate E_{opt}. The optical band gap of bulk $(BA)_2PbI_4$ is computed as 2.41 eV, which agrees very well with the experimental value of 2.43 eV.[32,33] The exciton binding energy is defined as $E_b = E_g - E_{opt}$, which is 0.34 eV for $(BA)_2PbI_4$, 10 times greater than K_BT. Similar calculations are carried out for bulk $(BA)_2PbCl_4$

DOI: 10.1021/acs.jpclett.9b01093
J. Phys. Chem. Lett. 2019, 10, 3820−3827

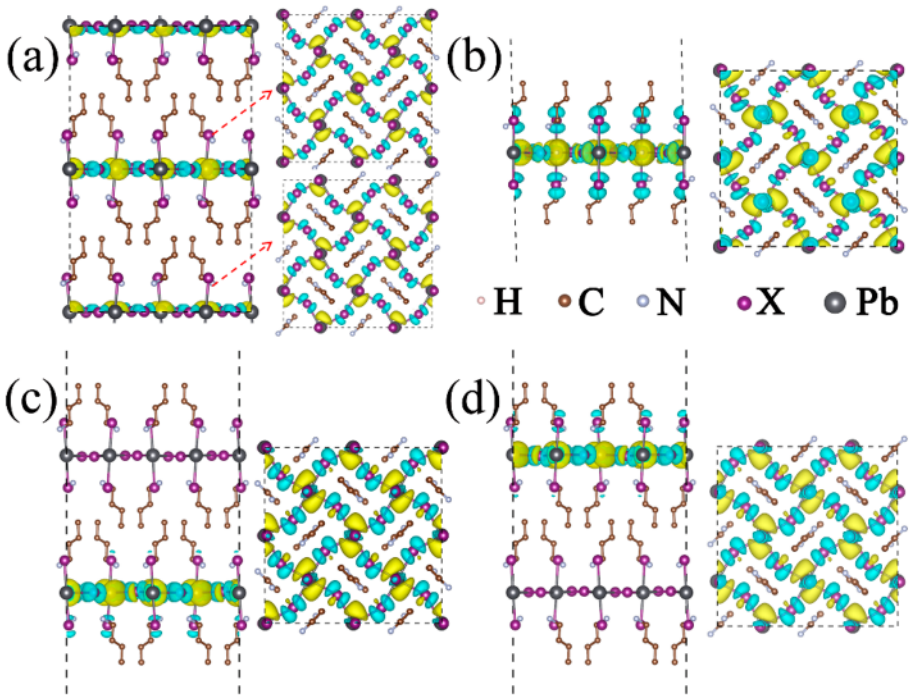

Figure 2. Side and top views of the exciton charge density in (a) bulk, (b) SL, and (c and d) DL $(BA)_2PbI_4$. The charge density of the electron and the hole is colored yellow and cyan, respectively. The isosurface level is set at 0.0003 e $bohr^{-3}$.

and $(BA)_2PbBr_4$, and we obtain an E_{opt} of 3.48 eV for $(BA)_2PbCl_4$, which compares well to the experimental value of 3.65 eV,[33,57] and an E_{opt} of 2.93 eV for $(BA)_2PbBr_4$, very close to the experimental value of 2.97 eV.[30,33,58] We have also determined E_{opt} values for the SL and DL of $(BA)_2PbX_4$ (X = Cl, Br, or I) and found that E_{opt} is slightly blue-shifted compared to the bulk value, consistent with the experimental observations.[33] Finally, as X varies from Cl to Br to I, the energy gaps and exciton binding energy decrease as shown in Figure 1d, because of the increase in the level of dielectric screening. The calculated band gaps and exciton binding energies of SL, DL, and bulk $(BA)_2PbX_4$ (X = Cl, Br, or I) are summarized in Table 2S and Figures 1S−9S. Overall, we find that the (TD)DFT-OT-RSH method without SOC is capable of yielding accurate E_{opt} and E_b values for the 2D perovskites. Importantly, we have previously shown that the parameters α, β, and γ can be transferred to the same material in the presence of point defects as long as the defect concentration is not too high.[45,55] Hence, in the following study of point defects in $(BA)_2PbI_4$, we will use the same set of α, β, and γ values. We do not include SOC in the calculations for the following reasons. (1) SOC is believed to be rather small on the Gamma point[59] for which our (TD)DFT-OT-RSH calculations are performed. (2) We have shown above that reliable E_{opt} values can be obtained for the 2D perovskites without including SOC. Because we fit our computational parameters to the experimental E_g, E_b ($=E_g - E_{opt}$) can thus be determined accurately without SOC, as well. (3) We show in the Supporting Information that the charge density of the frontier orbitals (and thus the exciton charge density) at the Gamma point exhibits negligible differences with and without the SOC correction (Figure 10S). Because in this work we mainly focus on the exciton binding energy and charge density, the highly expensive SOC calculations are not essential for our purposes.

The (TD)DFT-OT-RSH method also enables us to examine the charge density of excitons, and in Figure 2, we show the charge density of the lowest-energy exciton in SL, DL, and bulk $(BA)_2PbI_4$. In all three cases, the electron (yellow) and hole (cyan) of the exciton are delocalized in the quantum well (PbI_4) layer, characteristic of a Mott−Wannier exciton. For DL $(BA)_2PbI_4$, two nearly degenerate states exist for the lowest-energy exciton (Figure 2c,d), one at each PbI_4 layer. The higher-energy excitons are also delocalized in the inorganic layer (Figure 3S). As in the case of 3D perovskites, the excited electron originates from and resides on Pb 6p orbitals while the hole stems from I 5p orbitals. This implies that Pb and I defects could modify the band gaps and, thus, the exciton properties, including the exciton binding energy and charge density. Finally, we note that E_b varies between 0.30 and 0.35 eV in SL, DL, and bulk $(BA)_2PbI_4$.

In the following, we turn our attention to point defects in $(BA)_2PbI_4$. Because SL $(BA)_2PbI_4$ exhibits excitonic properties similar to those of the DL and bulk phase, we will first focus on the SL to minimize the computational cost. Ten neutral point defects, including three vacancies (V_{Pb}, V_I, and V_{BA}), four substitutions (Pb_I, I_{Pb}, I_{BA}, and Pb_{BA}), and three antisite configurations (exchanging Pb and I), are considered. The formation energy of a defect depends on the chemical environment (i.e., chemical potential) in which it is formed, such as the presence of precursors, partial pressures, temperature, and other synthetic conditions. In this work, we calculate the formation energies (E_f) of the point defects as a function of I chemical potential (μ_I) using the PBE functional[49] with the D2 correction.[50] Note that the defect formation energy is a ground state property, and the PBE-D2 functional is known to yield reliable ground state energetics. There are 295−311 atoms in the computational slab model of SL $(BA)_2PbI_4$ depending on the defect type. We follow a method that has been previously applied to the 2D and 3D perovskites[60,61] (details are provided in Supporting Information). Because E_f depends linearly on μ_I, the maximum and minimum of E_f should be bound at the phase boundaries: $\mu_{Pb} + 2\mu_I =$

DOI: 10.1021/acs.jpclett.9b01093
J. Phys. Chem. Lett. 2019, 10, 3820−3827

$\Delta H(PbI_2)$, and $\mu_{Pb} + 2\mu_I = \Delta H[(BA)_2PbI_4] - 2\Delta H(BAI)$, where $\Delta H[(BA)_2PbI_4]$, $\Delta H(PbI_2)$, and $\Delta H(BAI)$ are the formation enthalpies of SL $(BA)_2PbI_4$, PbI_2, and BAI, respectively. On the basis of the PBE-D2 calculations, we have $\Delta H[(BA)_2PbI_4]$, $\Delta H(BAI)$, and $\Delta H(PbI_2)$ values of −11.99, −2.88, and −2.80 eV, respectively. Therefore, the formation energies of different defects at the two boundaries can be obtained, as shown in Figure 3. We find that the

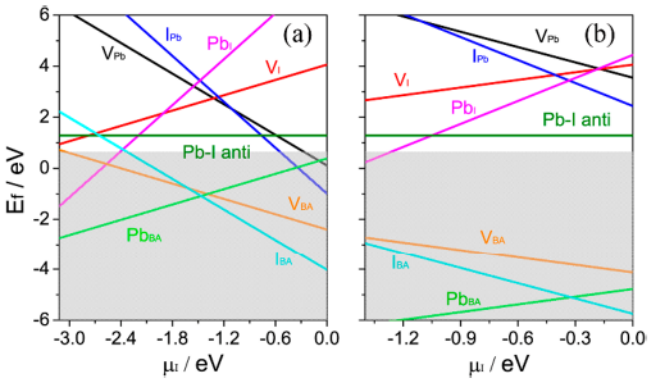

Figure 3. Formation energies of intrinsic point defects in SL $(BA)_2PbI_4$ as a function of μ_I at the phase boundaries: (a) $\mu_{Pb} + 2\mu_I = \Delta H[(BA)_2PbI_4] - 2\Delta H(BAI)$, and (b) $\mu_{Pb} + 2\mu_I = \Delta H(PbI_2)$.

dominant defects at high μ_I are those with surplus anions or deficient cations, such as V_{Pb}, I_{Pb}, I_{BA}, and V_{BA}. On the other hand, the cation surplus defect Pb_I has a lower formation energy at low μ_I values. It has been argued[60] that the defects with an E_f of ≲0.62 eV are likely to be formed under the normal experimental conditions (shaded area in Figure 3).[33] Thus, all defects examined here, with the exception of Pb−I antisite and V_I, are expected to be formed under the normal synthetic conditions. Specifically, the neutral lead vacancy V_{Pb} could be formed in an I-rich environment with a μ_I of greater than −0.3 eV. Note that the neutral lead vacancy was also found to have a low formation energy (∼0.29 eV) in 3D perovskite $MAPbI_3$ in an I-rich environment.[61]

We next examine the optoelectronic properties of the defective SL $(BA)_2PbI_4$. All known neutral and charged point defects have been examined, but some of them turn out to be metallic, which cannot be handled by the present (TD)DFT-OT-RSH method. Because we are interested in only semiconductors, the metallic defects are not included in our study. Among the included defects in Table 1, we find that most of them do not change E_b significantly with the exception of the neutral lead vacancy, V_{Pb}, which decreases E_b from 0.35 to 0.11 eV. This is a drastic decrease that could have important consequences in photovoltaic applications, as free carrier generation requires that E_b should be comparable to K_BT. As shown in Figure 2, the lowest-energy exciton in the pristine $(BA)_2PbI_4$ comprises a hole in I 5p orbitals and an electron in Pb 6p orbitals; i.e., the lowest excitation is from I 5p to Pb 6p. However, when a Pb atom is removed from the lattice, the nearby I ions lose two electrons that originated from the Pb atom. Thus, the highest occupied I 5p level is vacated, entering the band gap as shown in Figure 4a. As a result, the band gaps, E_g and E_{opt}, are decreased by >2.1 eV, and the lowest excitation is now between I 5p orbitals themselves. Note that the excited electron and hole are on different I ions and thus not localized in the same region (see Figures 5 and 6). In Figure 4b, we present the charge density of the lowest-energy exciton; the excited electron is delocalized throughout the inorganic layer, while the hole is localized at the Pb vacancy. To gain more insight, we examine the charge densities of three frontier orbitals obtained from the DFT calculations, including the lowest unoccupied molecule orbital (LUMO), the highest occupied molecular orbital (HOMO), and HOMO−1 (Figure 4c). We find that both LUMO and HOMO are delocalized while HOMO−1 is localized near the vacancy. These results suggest that the lowest-energy exciton is formed by an excitation from HOMO−1 to LUMO as opposed to that from HOMO to LUMO. The same conclusion can also be drawn by analyzing the orbital contributions to the wave function of the exciton. These results have an interesting implication. If the hole is elevated from HOMO−1 to HOMO, it will become delocalized. Indeed, we find delocalized excitons whose energies are only slightly higher than the lowest one, and two of them are shown in Figure 4d. The presence of delocalized excitons with a significantly decreased E_b suggests that free carriers can be generated more easily in SL $(BA)_2PbI_4$ in the presence of V_{Pb}, mitigating one of the crucial problems in $(BA)_2PbI_4$ for potential photovoltaics. Larger supercells with 701 and 1247 atoms have also been used to examine lower lead vacancy concentrations, and the results are shown in Figure 11S. Similar excitonic behavior is found in these systems.

Table 1. Calculated Fundamental (E_g) and Optical (E_{opt}) Band Gaps and Exciton Binding Energies (E_b) for SL $(BA)_2PbI_4$ in the Presence of Point Defects

defect	pristine	V_{Pb}	V_{Pb}''	I_{BA}	I_{BA}''	V_{BA}'	$Pb_{BA}^{\bullet}$	I_{Pb}'''
charge	0	0	−2	0	−2	−1	+1	−3
E_g (eV)	2.79	0.67	3.12	1.55	2.54	2.81	2.72	2.16
E_{opt} (eV)	2.45	0.56	2.77	1.26	2.32	2.46	2.41	N/A
E_b (eV)	0.34	0.11	0.35	0.29	0.22	0.35	0.31	N/A
description	no defect	neutral Pb vacancy	Pb^{2+} vacancy	I substitution for BA	I^- substitution for BA^+	BA^+ vacancy	Pb^{2+} substitution for BA^+	I^- substitution for Pb^{2+}

defect	$V_I^{\bullet}$ 1	$V_I^{\bullet}$ 2	$V_I^{\bullet}$ 3	$Pb_I^{\bullet\bullet\bullet}$ 1	$Pb_I^{\bullet\bullet\bullet}$ 2	$Pb_I^{\bullet\bullet\bullet}$ 3	antisite 1	antisite 2	antisite 3
charge	+1	+1	+1	+3	+3	+3	0	0	0
E_g (eV)	2.53	2.56	2.83	2.75	2.74	2.59	2.99	3.05	1.29
E_{opt} (eV)	2.22	2.25	2.49	2.44	2.44	2.30	2.68	2.73	1.06
E_b (eV)	0.31	0.31	0.34	0.31	0.30	0.29	0.31	0.32	0.23
description[a]	I_1^{-1} vacancy	I_2^{-1} vacancy	I_3^{-1} vacancy	Pb^{2+} substitution for I_1^{-1}	Pb^{2+} substitution for I_2^{-1}	Pb^{2+} substitution for I_3^{-1}	exchange between Pb and I_1^{-1}	exchange between Pb and I_2^{-1}	exchange between Pb and I_3^{-1}

[a]I ions are classified into three categories according to their non-equlivalent occupation sites labeled as I_1−I_3 in Figure 1e.

DOI: 10.1021/acs.jpclett.9b01093
J. Phys. Chem. Lett. 2019, 10, 3820−3827

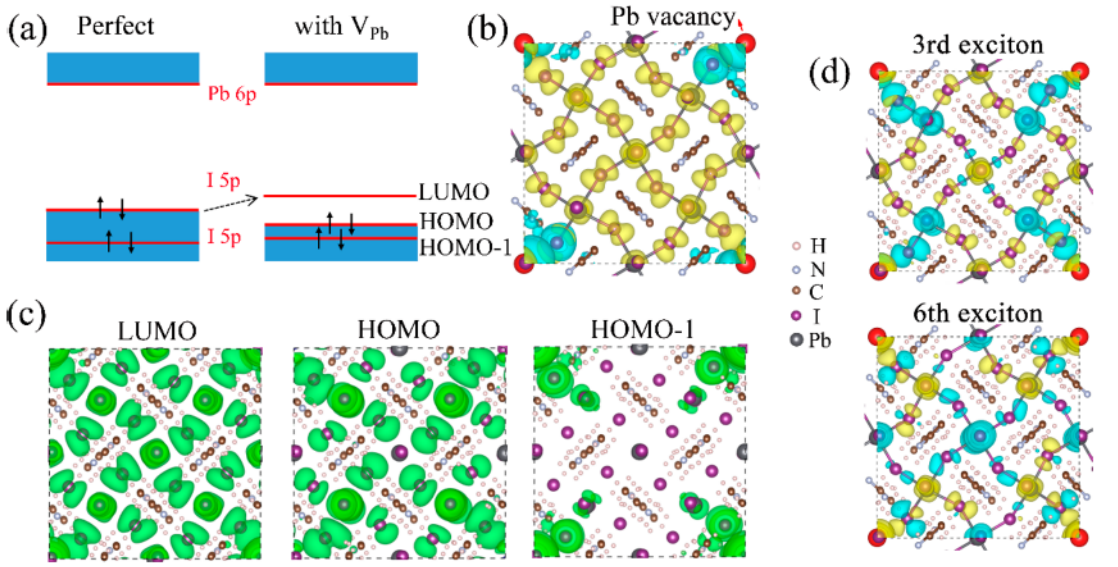

Figure 4. (a) Band diagrams of SL $(BA)_2PbI_4$ with and without lead vacancy V_{Pb}. (b) Charge density of the lowest-energy exciton in SL $(BA)_2PbI_4$ with the lead vacancy. (c) Charge densities of three frontier orbitals (LUMO, HOMO, and HOMO−1) in SL $(BA)_2PbI_4$ with the lead vacancy. (d) Charge densities of two higher-energy excitons (third and sixth) in SL $(BA)_2PbI_4$ with the lead vacancy. The lead vacancy is at the corners of the supercell represented by a red sphere. The supercell comprises 311 atoms. The charge density of the electron and the hole is colored yellow and cyan, respectively. The isosurface level is set at 0.0002 e bohr^{-3}.

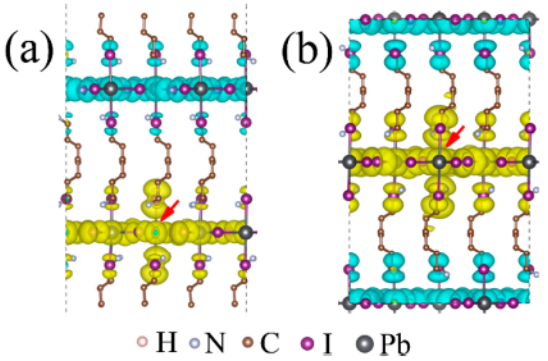

Figure 5. Charge densities of the lowest-energy exciton in (a) DL and (b) bulk $(BA)_2PbI_4$ with a lead vacancy (denoted by the red arrow). There are 623 atoms in the supercells for both systems. The charge density of the electron and the hole is colored yellow and cyan, respectively. The isosurface level is set at 0.0001 e bohr^{-3}.

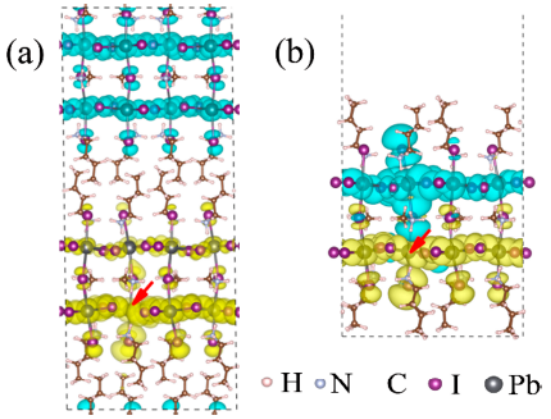

Figure 6. Charge densities of the lowest-energy exciton in the (a) bulk and (b) SL $(BA)_2(MA)Pb_2I_7$ with a lead vacancy denoted by a red arrow. The supercells contain 815 and 407 atoms, respectively. The charge density of the electron and the hole is colored yellow and cyan, respectively. The isosurface level is set at 0.0001 e bohr^{-3}.

To see whether the results in SL would hold for DL and bulk $(BA)_2PbI_4$, we performed similar calculations with a Pb vacancy introduced at one of the two inorganic layers in the DL phase and at every other inorganic layer in the bulk phase (shown in Figure 5a,b). The vacancy concentration in the bulk phase is estimated to be 1.3×10^{20} cm^{-3}. In both cases, we observe trends similar to those in the SL phase, i.e., large decreases in the band gaps and exciton binding energy. More specifically, we find $E_g = E_{opt} = 0.30$ eV and $E_b = 0.0$ eV in the DL phase and $E_g = 0.29$ eV, $E_{opt} = 0.26$ eV, and $E_b = 0.03$ eV in the bulk phase. More interestingly, the lowest-energy exciton is delocalized and the electron and hole are spatially separated; i.e., the electron delocalizes in the vacancy layer, while the hole spreads to the other layer. This charge separation is consistent with the fact that V_{Pb} is a dominant acceptor in the perovskites,[60,61] which attracts the electron and repels the hole. In addition, because V_{Pb} is a shallow defect, it does not lead to nonradiative charge recombination. Note that E_b is comparable to or smaller than the transition energy levels from the neutral to the charged vacancies in $MAPbI_3$;[61] thus, the exciton could dissociate into free carriers before the neutral vacancy makes transitions to the charged ones. In other words, if neutral Pb vacancies can be introduced into bulk $(BA)_2PbI_4$, they would yield spatially separated and delocalized charge carriers upon photoexcitation and hence promote charge generation (or suppress charge recombination) in the solar cells.

Finally, we extend the study to bulk $(BA)_2(MA)Pb_2I_7$, which is $n = 2$ equiv of $(BA)_2PbI_4$. $(BA)_2(MA)Pb_2I_7$ comprises of two quantum wells, each in turn consisting of two inorganic layers of octahedra (shown in Figure 6a). In the pristine bulk $(BA)_2(MA)Pb_2I_7$, we obtain $E_g = 2.5$ eV, $E_{opt} = 2.3$ eV, and $E_b = 0.2$ eV. Using a supercell of 815 atoms with a lead vacancy in the inorganic layer (the vacancy concentration is 8.4×10^{19} cm^{-3}), we find $E_g = 0.25$ eV, $E_{opt} = 0.22$ eV, and $E_b = 0.03$ eV for the bulk phase. As shown in Figure 6a, the excited electron

DOI: 10.1021/acs.jpclett.9b01093
J. Phys. Chem. Lett. 2019, 10, 3820−3827

and hole delocalize into the two separate quantum wells divided by the organic barriers. Again, the excited electron is attracted by the vacancy while the hole is repelled by it. SL $(BA)_2(MA)Pb_2I_7$ with a lead vacancy (Figure 6b) exhibits similar behavior with E_g = 0.24 eV, E_{opt} = 0.23 eV, and E_b = 0.01 eV.

For the bulk phase of $(BA)_2(MA)_{n-1}Pb_nX_{3n+1}$, we find E_b = 0.03 eV for both n = 1 and 2. This energy is comparable to K_BT; thus, free charge carriers can be readily generated in the presence of lead vacancies. Note that in our simulations, the vacancy concentration in $(BA)_2PbI_4$ is $\sim 1.3 \times 10^{20}$ cm^{-3}, almost doubling that in $(BA)_2(MA)Pb_2I_7$ ($\sim 8.4 \times 10^{19}$ cm^{-3}), but E_b is the same. Because of the computational constraints, the lowest vacancy concentration that we can examine is on the order of $10^{19}-10^{20}$ cm^{-3}. Walsh et al. have recently shown that the vacancy concentrations can actually reach this level in 3D $MAPbI_3$.[62] Therefore, we can consider a composite with defective regions embedded in the pristine material. The electronic structure (e.g., E_{opt} and E_b) of the pristine domain is only slightly perturbed by the defects; thus, light absorption should take place in the pristine domain and remain highly efficient. Once an exciton is generated, it cannot dissociate into free carriers because of its large binding energy. Thus, the exciton can only diffuse in the pristine domain, similar to the Frenkel excitons in organic photovoltaics (OPVs).[63−65] If the exciton reaches a defect region within its lifetime, it could dissociate into free carriers. One possible mechanism is illustrated in Figure 7, in which the "hot" electron of the exciton can relax to the defect LUMO level (see Figure 4a) via ultrafast energy transfer to the lattice vibrations. Simultaneously, the hole could occupy the defect HOMO level. As a result, the exciton becomes weakly bound and delocalized, which can then easily undergo dissociation into free carriers. Hence, the lead vacancies could play the role of bulk heterojunctions in OPVs, while ΔE plays the role of energetic driving force for charge separation.

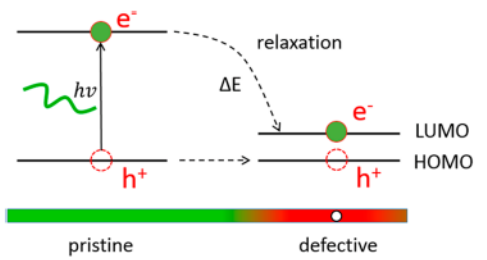

Figure 7. Schematic picture of exciton diffusion from the pristine to the defective region. The "hot" electron of the exciton relaxes to the LUMO level at the defect, losing its energy to the surrounding lattice. The hole would occupy the HOMO level at the defect.

With less atomic coordination, surfaces are usually sinks of vacancies. Thus, we expect higher concentrations of V_{Pb} at the surfaces of 2D perovskites, which could lead to a reduced E_b and more efficient carrier generation and/or slower charge recombination at the surfaces. Recent observation of long-lived free carriers at the edges of $(BA)_2(MA)_{n-1}Pb_nX_{3n+1}$ crystals (n = 1 and 2) implies that E_b could be reduced at the surfaces of the 2D perovskites.[22] However, the precise mechanism has yet to be elucidated. There is also an interesting experimental observation that 2D perovskite $PEA_2PbI_4{\cdot}(MAPbI_3)_{n-1}$ (PEA, phenethylammonium) with n = 2 exhibits charge recombination rates slower than those with n = 3 and 4.[66] We suspect that perhaps a large amount of Pb vacancies is present in the perovskite phase when n = 2.

In summary, we have studied electronic excitations in 2D perovskites $(BA)_2PbX_4$ (X = Cl, Br, or I) using the recently developed (TD)DFT-OT-RSH approach. We find red-shifts in the fundamental and optical band gaps as well as exciton binding energy as the halide varies from Cl to I. In SL, DL, and bulk $(BA)_2PbI_4$, excitons are delocalized in the inorganic slabs but with large E_b values. With SL as an example, we have calculated the formation energy of various point defects in $(BA)_2PbI_4$ as a function of I chemical potential. We predict that the neutral lead vacancies can decrease E_b significantly. The decrease in E_b is due to the fact that the excitation is no longer from I 5p to Pb 6p orbitals but rather between two I 5p orbitals. Similar results are also observed in DL and bulk $(BA)_2PbI_4$ as well as bulk $(BA)_2(MA)Pb_2I_7$ in which E_b is decreased to 0.03 eV, comparable to room temperature. Moreover, the excitons are predicted to be delocalized, with spatial separation between the electron and the hole. These results suggest that if Pb vacancies can be introduced into atomically thin $(BA)_2(MA)_{n-1}Pb_nX_{3n+1}$, they could yield spatially separated and delocalized charge carriers and thereby reduce charge recombination rates. Therefore, a major constraint of 2D perovskites for potential photovoltaic applications could be lifted. Our work paves the way for more stable and efficient photovoltaics based on 2D organic−inorganic halide perovskites.

■ ASSOCIATED CONTENT

Supporting Information

The Supporting Information is available free of charge on the ACS Publications website at DOI: 10.1021/acs.jpclett.9b01093.

Computational methods, calculated structural and key excitonic parameters of SL, DL, and bulk $(BA)_2PbX_4$, energies of formation of defects, and exciton distribution in $(BA)_2PbX_4$ (PDF)

■ AUTHOR INFORMATION

Corresponding Author

*E-mail: ganglu@csun.edu.

ORCID

Yurui Gao: 0000-0001-7486-8134
Mingliang Zhang: 0000-0002-7106-498X
Xu Zhang: 0000-0002-6491-3234

Notes

The authors declare no competing financial interest.

■ ACKNOWLEDGMENTS

The authors acknowledge the valuable discussion with Dr. Chongqin Zhu at the University of Pennsylvania. This work was supported by the NSF-PREM program (DMR1828019) and the Army Research Office (W911NF1810473).

■ REFERENCES

(1) Kojima, A.; Teshima, K.; Shirai, Y.; Miyasaka, T. Organometal Halide Perovskites as Visible-Light Sensitizers for Photovoltaic Cells. *J. Am. Chem. Soc.* **2009**, *131*, 6050−6051.

(2) Liao, H. C.; Tam, T. L. D.; Guo, P.; Wu, Y.; Manley, E. F.; Huang, W.; Zhou, N.; Soe, C. M. M.; Wang, B.; Wasielewski, M. R.; et al. Dopant-Free Hole Transporting Polymers for High Efficiency,

DOI: 10.1021/acs.jpclett.9b01093
J. Phys. Chem. Lett. 2019, 10, 3820−3827

Environmentally Stable Perovskite Solar Cells. *Adv. Energy Mater.* **2016**, *6*, 1600502.
(3) Nie, W.; Tsai, H.; Asadpour, R.; Blancon, J. C.; Neukirch, A. J.; Gupta, G.; Crochet, J. J.; Chhowalla, M.; Tretiak, S.; Alam, M. A.; et al. High-Efficiency Solution-Processed Perovskite Solar Cells with Millimeter-Scale Grains. *Science* **2015**, *347*, 522−525.
(4) Manser, J. S.; Christians, J. A.; Kamat, P. V. Intriguing Optoelectronic Properties of Metal Halide Perovskites. *Chem. Rev.* **2016**, *116*, 12956−13008.
(5) Huang, J.; Yuan, Y.; Shao, Y.; Yan, Y. Understanding the Physical Properties of Hybrid Perovskites for Photovoltaic Applications. *Nat. Rev. Mater.* **2017**, *2*, 17042.
(6) Liu, B.; Soe, C. M. M.; Stoumpos, C. C.; Nie, W.; Tsai, H.; Lim, K.; Mohite, A. D.; Kanatzidis, M. G.; Marks, T. J.; Singer, K. D. Optical Properties and Modeling of 2D Perovskite Solar Cells. *Sol. RRL* **2017**, *1*, 1700062.
(7) Tan, Z.; Wu, Y.; Hong, H.; Yin, J.; Zhang, J.; Lin, L.; Wang, M.; Sun, X.; Sun, L.; Huang, Y.; et al. Two-Dimensional $(C_4H_9NH_3)_2PbBr_4$ Perovskite Crystals for High-Performance Photodetector. *J. Am. Chem. Soc.* **2016**, *138*, 16612−16615.
(8) Chin, X. Y.; Cortecchia, D.; Yin, J.; Bruno, A.; Soci, C. Lead Iodide Perovskite Light-Emitting Field-Effect Transistor. *Nat. Commun.* **2015**, *6*, 7383.
(9) Li, F.; Ma, C.; Wang, H.; Hu, W.; Yu, W.; Sheikh, A. D.; Wu, T. Ambipolar Solution-Processed Hybrid Perovskite Phototransistors. *Nat. Commun.* **2015**, *6*, 8238.
(10) Tan, Z. K.; Moghaddam, R. S.; Lai, M. L.; Docampo, P.; Higler, R.; Deschler, F.; Price, M.; Sadhanala, A.; Pazos, L. M.; Credgington, D.; et al. Bright Light-Emitting Diodes Based on Organometal Halide Perovskite. *Nat. Nanotechnol.* **2014**, *9*, 687−692.
(11) Fang, Y.; Dong, Q.; Shao, Y.; Yuan, Y.; Huang, J. Highly Narrowband Perovskite Single-Crystal Photodetectors Enabled by Surface-Charge Recombination. *Nat. Photonics* **2015**, *9*, 679−686.
(12) Jiang, Q.; Chu, Z.; Wang, P.; Yang, X.; Liu, H.; Wang, Y.; Yin, Z.; Wu, J.; Zhang, X.; You, J. Planar-Structure Perovskite Solar Cells with Efficiency Beyond 21%. *Adv. Mater.* **2017**, *29*, 1703852.
(13) Green, M. A.; Hishikawa, Y.; Dunlop, E. D.; Levi, D. H.; Hohl-Ebinger, J.; Yoshita, M.; Ho-Baillie, A. W. Y. Solar Cell Efficiency Tables (Version 53). *Prog. Photovoltaics* **2019**, *27*, 3−12.
(14) Baikie, T.; Fang, Y.; Kadro, J. M.; Schreyer, M.; Wei, F.; Mhaisalkar, S. G.; Graetzel, M.; White, T. J. Synthesis and Crystal Chemistry of the Hybrid Perovskite $(CH_3NH_3)PbI_3$ for Solid-State Sensitised Solar Cell Applications. *J. Mater. Chem. A* **2013**, *1*, 5628−5641.
(15) Divitini, G.; Cacovich, S.; Matteocci, F.; Cinà, L.; Di Carlo, A.; Ducati, C. In Situ Observation of Heat-Induced Degradation of Perovskite Solar Cells. *Nat. Energy* **2016**, *1*, 15012.
(16) Stoumpos, C. C.; Malliakas, C. D.; Kanatzidis, M. G. Semiconducting Tin and Lead Iodide Perovskites with Organic Cations: Phase Transitions, High Mobilities, and near-Infrared Photoluminescent Properties. *Inorg. Chem.* **2013**, *52*, 9019−9038.
(17) Niu, G.; Guo, X.; Wang, L. Review of Recent Progress in Chemical Stability of Perovskite Solar Cells. *J. Mater. Chem. A* **2015**, *3*, 8970−8980.
(18) Cao, D. H.; Stoumpos, C. C.; Farha, O. K.; Hupp, J. T.; Kanatzidis, M. G. 2D Homologous Perovskites as Light-Absorbing Materials for Solar Cell Applications. *J. Am. Chem. Soc.* **2015**, *137*, 7843−7850.
(19) Grancini, G.; Roldan-Carmona, C.; Zimmermann, I.; Mosconi, E.; Lee, X.; Martineau, D.; Narbey, S.; Oswald, F.; De Angelis, F.; Graetzel, M.; Nazeeruddin, M. K. One-Year Stable Perovskite Solar Cells by 2D/3D Interface Engineering. *Nat. Commun.* **2017**, *8*, 15684.
(20) Smith, I. C.; Hoke, E. T.; Solis-Ibarra, D.; McGehee, M. D.; Karunadasa, H. I. A Layered Hybrid Perovskite Solar-Cell Absorber with Enhanced Moisture Stability. *Angew. Chem., Int. Ed.* **2014**, *53*, 11232−11235.
(21) Tsai, H. H.; Nie, W.; Blancon, J. C.; Stoumpos, C. C.; Asadpour, R.; Harutyunyan, B.; Neukirch, A. J.; Verduzco, R.; Crochet, J. J.; Tretiak, S.; et al. High-Efficiency Two-Dimensional Ruddlesden-Popper Perovskite Solar Cells. *Nature* **2016**, *536*, 312−316.
(22) Blancon, J. C.; Tsai, H.; Nie, W.; Stoumpos, C. C.; Pedesseau, L.; Katan, C.; Kepenekian, M.; Soe, C. M. M.; Appavoo, K.; Sfeir, M. Y.; et al. Extremely Efficient Internal Exciton Dissociation through Edge States in Layered 2D Perovskites. *Science* **2017**, *355*, 1288−1292.
(23) Wang, Z.; Lin, Q.; Chmiel, F. P.; Sakai, N.; Herz, L. M.; Snaith, H. J. Efficient Ambient-Air-Stable Solar Cells with 2D-3D Heterostructured Butylammonium-Caesium-Formamidinium Lead Halide Perovskites. *Nat. Energy* **2017**, *2*, 17135.
(24) Grancini, G.; Nazeeruddin, M. K. Dimensional Tailoring of Hybrid Perovskites for Photovoltaics. *Nat. Rev. Mater.* **2019**, *4*, 4−22.
(25) Takeoka, Y.; Asai, K.; Rikukawa, M.; Sanui, K. Systematic Studies on Chain Lengths, Halide Species, and Well Thicknesses for Lead Halide Layered Perovskite Thin Films. *Bull. Chem. Soc. Jpn.* **2006**, *79*, 1607−1613.
(26) Stoumpos, C. C.; Cao, D. H.; Clark, D. J.; Young, J.; Rondinelli, J. M.; Jang, J. I.; Hupp, J. T.; Kanatzidis, M. G. Ruddlesden-Popper Hybrid Lead Iodide Perovskite 2D Homologous Semiconductors. *Chem. Mater.* **2016**, *28*, 2852−2867.
(27) Chen, Y.; Sun, Y.; Peng, J.; Tang, J.; Zheng, K.; Liang, Z. 2D Ruddlesden-Popper Perovskites for Optoelectronics. *Adv. Mater.* **2018**, *30*, 1703487.
(28) Wang, N.; Cheng, L.; Ge, R.; Zhang, S.; Miao, Y.; Zou, W.; Yi, C.; Sun, Y.; Cao, Y.; Yang, R.; et al. Perovskite Light-Emitting Diodes Based on Solution-Processed Self-Organized Multiple Quantum Wells. *Nat. Photonics* **2016**, *10*, 699−704.
(29) Saidaminov, M. I.; Mohammed, O. F.; Bakr, O. M. Low-Dimensional-Networked Metal Halide Perovskites: the Next Big Thing. *ACS Energy Lett.* **2017**, *2*, 889−896.
(30) Kitazawa, N.; Aono, M.; Watanabe, Y. Excitons in Organic-Inorganic Hybrid Compounds $(C_nH_{2n+1}NH_3)_2PbBr_4$ (n = 4, 5, 7 and 12). *Thin Solid Films* **2010**, *518*, 3199−3203.
(31) Blancon, J. C.; Stier, A. V.; Tsai, H.; Nie, W.; Stoumpos, C. C.; Traoré, B.; Pedesseau, L.; Kepenekian, M.; Katsutani, F.; Noe, G. T.; et al. Scaling Law for Excitons in 2D Perovskite Quantum Wells. *Nat. Commun.* **2018**, *9*, 2254.
(32) Amerling, E.; Baniya, S.; Lafalce, E.; Zhang, C.; Vardeny, Z. V.; Whittaker-Brooks, L. Electroabsorption Spectroscopy Studies of $(C_4H_9NH_3)_2PbI_4$ Organic-Inorganic Hybrid Perovskite Multiple Quantum Wells. *J. Phys. Chem. Lett.* **2017**, *8*, 4557−4564.
(33) Dou, L.; Wong, A. B.; Yu, Y.; Lai, M.; Kornienko, N.; Eaton, S. W.; Fu, A.; Bischak, C. G.; Ma, J.; Ding, T.; et al. Atomically Thin Two-Dimensional Organic-Inorganic Hybrid Perovskites. *Science* **2015**, *349*, 1518−1521.
(34) Lin, Q.; Armin, A.; Nagiri, R. C. R.; Burn, P. L.; Meredith, P. Electro-Optics of Perovskite Solar Cells. *Nat. Photonics* **2015**, *9*, 106−112.
(35) Menéndez-Proupin, E.; Palacios, P.; Wahnón, P.; Conesa, J. C. Self-Consistent Relativistic Band Structure of the $CH_3NH_3PbI_3$ Perovskite. *Phys. Rev. B: Condens. Matter Mater. Phys.* **2014**, *90*, 045207.
(36) D'Innocenzo, V.; Grancini, G.; Alcocer, M. J. P.; Kandada, A. R. S.; Stranks, S. D.; Lee, M. M.; Lanzani, G.; Snaith, H. J.; Petrozza, A. Excitons Versus Free Charges in Organo-Lead Tri-Halide Perovskites. *Nat. Commun.* **2014**, *5*, 3586.
(37) Hirasawa, M.; Ishihara, T.; Goto, T.; Uchida, K.; Miura, N. Magnetoabsorption of the Lowest Exciton in Perovskite-Type Compound $(CH_3NH_3)PbI_3$. *Phys. B* **1994**, *201*, 427−430.
(38) Hong, X.; Ishihara, T.; Nurmikko, A. V. Dielectric Confinement Effect on Excitons in PbI_4-Based Layered Semiconductors. *Phys. Rev. B: Condens. Matter Mater. Phys.* **1992**, *45*, 6961−6964.
(39) Wang, D.; Wen, B.; Zhu, Y. N.; Tong, C. J.; Tang, Z. K.; Liu, L. M. First-Principles Study of Novel Two-Dimensional $(C_4H_9NH_3)_2PbX_4$ Perovskites for Solar Cell Absorbers. *J. Phys. Chem. Lett.* **2017**, *8*, 876−883.
(40) Hybertsen, M. S.; Louie, S. G. Electron Correlation in Semiconductors and Insulators: Band Gaps and Quasiparticle

DOI: 10.1021/acs.jpclett.9b01093
J. Phys. Chem. Lett. 2019, 10, 3820−3827

Energies. *Phys. Rev. B: Condens. Matter Mater. Phys.* **1986**, *34*, 5390−5413.
(41) Salpeter, E. E.; Bethe, H. A. A Relativistic Equation for Bound-State Problems. *Phys. Rev.* **1951**, *84*, 1232−1242.
(42) Rohlfing, M.; Louie, S. G. Electron-Hole Excitations in Semiconductors and Insulators. *Phys. Rev. Lett.* **1998**, *81*, 2312−2315.
(43) Becke, A. D. A. New Mixing of Hartree-Fock and Local Density-Functional Theories. *J. Chem. Phys.* **1993**, *98*, 1372−1377.
(44) Liu, Z. F.; Egger, D. A.; Refaely-Abramson, S.; Kronik, L.; Neaton, J. B. Energy Level Alignment at Molecule-Metal Interfaces from an Optimally Tuned Range-Separated Hybrid Functional. *J. Chem. Phys.* **2017**, *146*, 092326.
(45) Huang, L. Y.; Zhang, X.; Zhang, M.; Lu, G. Effect of Point Defects on Optical Properties of Graphene Fluoride: A First-Principles Study. *J. Phys. Chem. C* **2017**, *121*, 12855−12862.
(46) Refaely-Abramson, S.; Jain, M.; Sharifzadeh, S.; Neaton, J. B.; Kronik, L. Solid-State Optical Absorption from Optimally Tuned Time-Dependent Range-Separated Hybrid Density Functional Theory. *Phys. Rev. B: Condens. Matter Mater. Phys.* **2015**, *92*, 081204.
(47) Kronik, L.; Neaton, J. B. Excited-State Properties of Molecular Solids from First Principles. *Annu. Rev. Phys. Chem.* **2016**, *67*, 587−616.
(48) Refaely-Abramson, S.; Sharifzadeh, S.; Jain, M.; Baer, R.; Neaton, J. B.; Kronik, L. Gap Renormalization of Molecular Crystals from Density-Functional Theory. *Phys. Rev. B: Condens. Matter Mater. Phys.* **2013**, *88*, 081204.
(49) Perdew, J. P.; Burke, K.; Ernzerhof, M. Generalized Gradient Approximation Made Simple. *Phys. Rev. Lett.* **1996**, *77*, 3865−3868.
(50) Grimme, S. Semiempirical GGA-Type Density Functional Constructed with a Long-Range Dispersion Correction. *J. Comput. Chem.* **2006**, *27*, 1787−1799.
(51) Mitzi, D. B. Synthesis, Crystal Structure, and Optical and Thermal Properties of $(C_4H_9NH_3)_2MI_4$ (M = Ge, Sn, Pb). *Chem. Mater.* **1996**, *8*, 791−800.
(52) Pedesseau, L.; Kepenekian, M.; Sapori, D.; Huang, Y.; Rolland, A.; Beck, A.; Cornet, C.; Durand, O.; Wang, S.; Katan, C.; Even, J. Dielectric Properties of Hybrid Perovskites and Drift-Diffusion Modeling of Perovskite Cells. *Proc. SPIE* **2016**, *9743*, 97430N.
(53) Onoda-Yamamuro, N.; Matsuo, T.; Suga, H. Dielectric Study of $CH_3NH_3PbX_3$ (X = Cl, Br, I). *J. Phys. Chem. Solids* **1992**, *53*, 935−939.
(54) Brivio, F.; Walker, A. B.; Walsh, A. Structural and Electronic Properties of Hybrid Perovskites for High-Efficiency Thin-Film Photovoltaics from First-Principles. *APL Mater.* **2013**, *1*, 042111.
(55) Huang, L. Y.; Zhang, X.; Zhang, M.; Lu, G. Optically Inactive Defects in Monolayer and Bilayer Phosphorene: A First-Principles Study. *Phys. Rev. Mater.* **2018**, *2*, 054003.
(56) Nan, G.; Zhang, X.; Abdi-Jalebi, M.; Andaji-Garmaroudi, Z.; Stranks, S. D.; Lu, G.; Beljonne, D. How Methylammonium Cations and Chlorine Dopants Heal Defects in Lead Iodide Perovskites. *Adv. Energy Mater.* **2018**, *8*, 1702754.
(57) Calabrese, J.; Jones, N. L.; Harlow, R. L.; Herron, N.; Thorn, D. L.; Wang, Y. Preparation and Characterization of Layered Lead Halide Compounds. *J. Am. Chem. Soc.* **1991**, *113*, 2328−2330.
(58) Tanaka, K.; Takahashi, T.; Kondo, T.; Umeda, K.; Ema, K.; Umebayashi, T.; Asai, K.; Uchida, K.; Miura, N. Electronic and Excitonic Structures of Inorganic-Organic Perovskite-Type Quantum-Well Crystal $(C_4H_9NH_3)_2PbBr_4$. *Jpn. J. Appl. Phys.* **2005**, *44*, 5923−5932.
(59) Mosconi, E.; Etienne, T.; De Angelis, F. Rashba Band Splitting in Organohalide Lead Perovskites: Bulk and Surface Effects. *J. Phys. Chem. Lett.* **2017**, *8*, 2247−2252.
(60) Liu, Y.; Xiao, H.; Goddard, W. A. Two-Dimensional Halide Perovskites: Tuning Electronic Activities of Defects. *Nano Lett.* **2016**, *16*, 3335−3340.
(61) Yin, W. J.; Shi, T.; Yan, Y. Unusual Defect Physics in $CH_3NH_3PbI_3$ Perovskite Solar Cell Absorber. *Appl. Phys. Lett.* **2014**, *104*, 063903.
(62) Walsh, A.; Scanlon, D. O.; Chen, S.; Gong, X. G.; Wei, S. H. Self-Regulation Mechanism for Charged Point Defects in Hybrid Halide Perovskites. *Angew. Chem., Int. Ed.* **2015**, *54*, 1791−1794.
(63) Mikhnenko, O. V.; Blom, P. W. M.; Nguyen, T. Q. Exciton Diffusion in Organic Semiconductors. *Energy Environ. Sci.* **2015**, *8*, 1867−1888.
(64) Zhang, X.; Li, Z.; Lu, G. First-Principles Simulations of Exciton Diffusion in Organic Semiconductors. *Phys. Rev. B: Condens. Matter Mater. Phys.* **2011**, *84*, 235208.
(65) Li, Z.; Zhang, X.; Woellner, C. F.; Lu, G. Understanding Molecular Structure Dependence of Exciton Diffusion in Conjugated Small Molecules. *Appl. Phys. Lett.* **2014**, *104*, 143303.
(66) Chen, X.; Lu, H.; Li, Z.; Zhai, Y.; Ndione, P. F.; Berry, J. J.; Zhu, K.; Yang, Y.; Beard, M. C. Impact of Layer Thickness on the Charge Carrier and Spin Coherence Lifetime in Two-Dimensional Layered Perovskite Single Crystals. *ACS Energy Lett.* **2018**, *3*, 2273−2279.

DOI: 10.1021/acs.jpclett.9b01093
J. Phys. Chem. Lett. 2019, 10, 3820−3827